Research Article BEU Fen Bilimleri Dergisi 15(1): 267-287 (2026) DOI: 10.17798/bitlisfen.1798886

BİTLİS EREN UNIVERSITY
FEN BİLİMLERİ DERGİSİ
ISSN: 2147-3129 / e-ISSN: 2147-3188

A HYBRID FINITE ELEMENT AND ADAPTIVE FUZZY LOGIC APPROACH FOR OPTIMIZING NANO-ENHANCED HEAT EXCHANGERS

Taha Kubilay ŞENER[1], Ali TAŞKIRAN [2], **Gülşah ÇAKMAK** [3*]

[1] *Fırat University, Computer Engineering Department, Elazığ, Türkiye*
[2] *Şırnak University, Mechanical Engineering Department, Şırnak, Türkiye*
[3] *Fırat University, Mechanical Engineering Department, Elazığ, Türkiye*
**** Corresponding Author:*** *gulcakmak@firat.edu.tr*

Article Info

Received: *October 8, 2025*
Revised: *December 22, 2025*
Accepted: *January 12, 2026*

Keywords
U-tube heat exchanger,
Phase Change Materials (PCMs),
Nanoparticle-enhanced PCM,
ANFIS,
Optimization,
Surrogate model.

ABSTRACT

This work investigates approaches to enhance the thermal performance of U-tube heat exchangers by coupling them with phase change materials (PCMs) enhanced with Al_2O_3 nanoparticles. The focus is on investigating how nanoparticle addition and wavy tube configurations influence the melting behavior. A numerical finite element model was validated against a reference study, confirming its accuracy. The incorporation of Al_2O_3 nanoparticles (0%, 1%, and 2%) led to a substantial improvement, reducing melting times by up to 80%. Notably, the wavy tube system with 2% nanoparticle-enhanced PCM demonstrated superior performance. To circumvent the significant computational expense associated with finite element analysis, an Adaptive Network-Based Fuzzy Inference System (ANFIS) was employed as a surrogate model. With a high prediction accuracy ($R^2 > 0.997$) for melting dynamics, the ANFIS model was then employed for a detailed optimization analysis. The optimization identified an ideal nanoparticle concentration of 3.50%, which minimizes the melting time to 263.63 seconds under wavy tube conditions. The findings underscore the potential of a hybrid FEA-ANFIS methodology, suggesting that a synergistic combination of nanotechnology, advanced geometries, and artificial intelligence offers an effective approach to improving the design and operational efficiency of thermal energy storage units.

1. INTRODUCTION

In industries ranging from power generation to HVAC systems, where effective thermal management is paramount, shell-and-tube heat exchangers are a core technology. Optimizing thermal regulation plays a key role in enhancing performance and improving energy efficiency. The capacity of PCMs to manage large thermal loads has made them a key technology, particularly as interest in sustainable energy solutions grows. Through latent heat storage, PCMs offer high energy capacity while maintaining a stable temperature during phase transitions, contributing to effective thermal control.

The widespread adoption of PCMs is primarily constrained by a single material property: their low thermal conductivity. This characteristic poses a significant design challenge, particularly in applications where rapid thermal response is critical. To overcome this limitation, researchers have explored the incorporation of nanoparticles into PCMs to create nano-enhanced PCMs (nanoPCMs), thereby improving their thermal performance. Advances in nanotechnology have introduced innovative solutions for improving thermal energy storage systems. In particular, these colloidal suspensions show superior thermal conductivity compared to conventional fluids. This enhancement has been extensively investigated for integration with PCMs to optimize heat transfer efficiency, showing promising results in improving heat exchanger performance.

Several studies have investigated ways to improve the efficiency of thermal energy systems. For instance, Maghsoudali et al. [1] analyzed finned configurations, while Fadaei et al. [2] explored how

tube arrangement impacts the melting process. Similarly, a recent comprehensive study by Su et al. [3] combined experimental and numerical methods to analyze the melting behavior in conventional shell and tube latent heat storage units, which provide a strong baseline for evaluating advanced designs. Furthermore, studies like that of Berent, Cihan, and Demir [4], which examined the thermal behavior of PCMs in 2D plates and showed strong agreement between numerical and analytical models, highlight the growing potential and reliability of modeling PCMs in energy storage applications. In addition, advancements in materials science, such as the use of GFRP reinforcements analyzed by Alharthi et al. [5], highlight the value of integrating advanced materials into engineering systems. Following this trend, the integration of inorganic PCMs like $CaCl_2 \cdot 6H_2O$ into U-tube heat exchangers (UHEs) has been studied for their high thermal storage potential. However, the inherently low thermal conductivity of such PCMs remains a bottleneck.

While previous studies have explored either the use of nano-enhanced PCMs [1, 2] or modified geometries [4] individually, a significant gap remains in understanding their synergistic effects and efficiently optimizing the combined design. This study addresses this gap through a multi-faceted approach, presenting three key contributions . First, it provides a comprehensive numerical analysis of the combined impact of Al_2O_3 nanoparticles and an innovative wavy tube geometry on the thermal performance of a U-tube heat exchanger. Second, to overcome the prohibitive computational cost of traditional simulation-based optimization, this work introduces a hybrid FEA-ANFIS methodology. This approach aligns with the growing trend of using AI-based surrogate models in thermal energy storage, a field extensively reviewed by Mehraj et al. [6]. By leveraging a high-fidelity Finite Element Analysis (FEA) model to generate a reliable dataset, we train a computationally efficient and accurate Adaptive Network-Based Fuzzy Inference System (ANFIS), originally proposed by Jang [7], to serve as a surrogate model. Third, the developed ANFIS model is then utilized to perform a rapid and detailed optimization, identifying the optimal nanoparticle concentration that minimizes melting time—a task impractical with FEA alone. This integration of numerical simulation, advanced geometry, nanotechnology, and artificial intelligence provides a novel and powerful framework for designing advanced thermal energy storage systems.

2. PROBLEM STATEMENT AND METHODOLOGY

Figure 1 presents the schematic diagram and dimensional details of the UHE utilized in the charging process of thermal energy storage systems. The system consists of a central body, which houses the wavy tubes, and an outer casing that encloses the PCM mixture. The UHE design is optimized to facilitate efficient heat transfer by ensuring that the hot fluid passes through the wavy tubes, creating turbulence and enhancing heat exchange with the PCM.

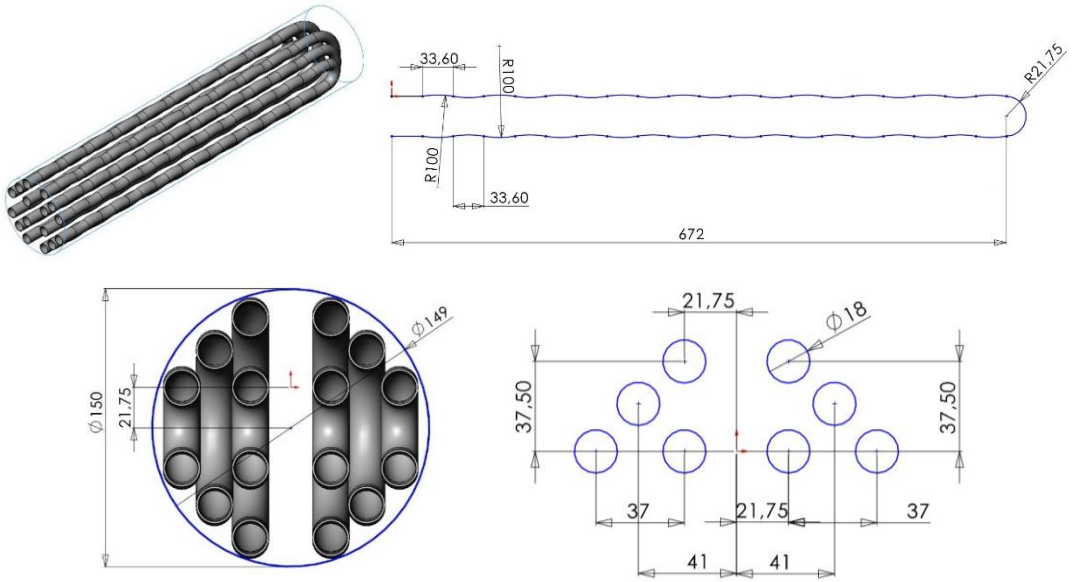

Figure 1. Wavy U-tube heat exchanger

During the charging process, hot fluid is circulated through the wavy tubes, which are positioned within the main body of the heat exchanger. The space between the wavy tubes and the surrounding outer casing serves as the thermal storage zone, where the PCM—composed of $CaCl_6H_2O$ combined with Al_2O_3 nanoparticles—is contained. When the hot fluid transfers heat to the PCM, the material undergoes a phase change, storing thermal energy. The wavy tube design is crucial for enhancing heat transfer efficiency by improving fluid mixing and reducing thermal boundary layers, which in turn accelerates the heat absorption process by the PCM.

The addition of Al_2O_3 nanoparticles to the PCM further enhances its thermal conductivity, allowing for a faster phase change process and more efficient thermal energy storage. The design and configuration of the wavy tubes are crucial in optimizing the performance of the UHE, as they contribute to uniform heat distribution, thereby reducing the likelihood of hotspots and ensuring a more effective thermal charging cycle. This system design is particularly well-suited for applications that require rapid thermal response and high energy storage densities, making it a promising candidate for advanced thermal management in energy systems.

2.1. Fundamental Equations Used

To investigate the melting behavior of nanoPCM within the UHE, this study utilizes a numerical model founded on the governing principles of heat transfer, fluid dynamics, and phase transition. These equations play a crucial role in accurately modeling the thermal behavior of the system and predicting its overall performance.

The model's foundation is the energy conservation principle, which is formulated separately for the working fluid and the phase change material. For the fluid, the energy balance considers the heat exchange occurring between the flowing hot fluid and the surrounding nanoPCM. The temperature distribution of the fluid is primarily governed by convective heat transfer and can be expressed as [8]:

$$\rho_f c_p \frac{\partial T_f}{\partial t} + \nabla \cdot (\rho_f c_p \vec{u}(T_f - T_\infty)) = \nabla \cdot (k_f \nabla T_f) \tag{1}$$

Within Equation (1), the terms ρf, cp, and Tf correspond to the fluid's density, specific heat capacity, and temperature, respectively, while the vector u represents the fluid velocity. This formulation takes into account both conductive and convective heat transfer within the fluid and the thermal energy transfer to the surrounding nanoPCM.

The phase transition process of the PCM is modeled using the Stefan problem, which describes the movement of the phase change boundary as a result of the heat absorbed. The rate of the solid-to-liquid phase transition within the PCM is directly governed by its latent heat of fusion. The energy equation governing the PCM's behavior during this phase change can be expressed as [9]:

$$\rho_{PCM} c_p \frac{\partial T_{PCM}}{\partial t} + \nabla \cdot (k_{PCM} \nabla T_{PCM}) = \lambda \frac{\partial m}{\partial t} \tag{2}$$

In this equation, ρ_{PCM} denotes the density of the PCM, cp is its specific heat capacity, T_{PCM} is the PCM's temperature, k_{PCM} represents its thermal conductivity, and λ stands for the latent heat of fusion. The term m represents the local liquid fraction, a dimensionless quantity that ranges from 0 for a fully solid material to 1 for a fully liquid material. The term $\partial m/\partial t$ represents the rate of phase change, which is crucial for accurately modeling both melting and solidification phases.

Adding Al_2O_3 nanoparticles to the PCM enhances its thermal conductivity, which in turn affects the phase transition properties. The enhanced thermal properties of the composite material are evaluated using effective medium approximations or models such as the Hamilton-Crosser correlation. This improvement in thermal conductivity enhances heat transfer efficiency, leading to a faster melting process.

Additionally, the Navier-Stokes equations are employed to describe the fluid dynamics within the wavy tube configuration, considering the velocity field and pressure variations that impact convective heat transfer. The governing equation for momentum conservation in the fluid domain is formulated as [8]:

$$\rho_f \left(\frac{\partial \vec{u}}{\partial t} + \vec{u} \cdot \nabla \vec{u} \right) = -\nabla P + \mu_f \nabla^2 \vec{u} \tag{3}$$

where P is the pressure field and μ_f is the dynamic viscosity of the fluid. This equation, coupled with the energy and continuity equations, governs the convective transport and flow behavior inside the heat exchanger.

By solving these interconnected equations, the thermal response and phase transition characteristics of the nanoPCM within the UHE can be effectively analyzed. This approach provides critical insights into the efficiency of the heat exchanger and the overall phase change dynamics. These mathematical formulations form the basis of the numerical model, which is validated against experimental findings to confirm its accuracy and applicability in practical scenarios.

Applying these governing equations enables a thorough evaluation of the melting process and thermal behavior of the nanoPCM-integrated heat exchanger. This, in turn, supports the refinement of thermal energy storage technologies, contributing to enhanced system performance and energy efficiency.

The enthalpy of the nanoPCM throughout the phase transition is determined using the following formulation, which accounts for both sensible and latent heat contributions:

$$H = \int_{T_0}^{T} c_p(T)\, dT + \lambda m \tag{4}$$

In this equation, H denotes the enthalpy, T_0 is the initial temperature, T is the current temperature, $c_p(T)$ is the specific heat capacity that varies with temperature, and m represents the mass of the phase change material (PCM) undergoing the phase transition. The second term, λm, represents the latent heat involved in the phase transition, where λ denotes the latent heat of fusion, and m corresponds to the mass of the substance undergoing the phase change.

To accurately model the thermal behavior of PCMs during phase transitions, enthalpy is utilized as a vital parameter for assessing energy storage and release. The enthalpy of nanoPCM, incorporating Al_2O_3 nanoparticles, is evaluated for both solid and liquid states as temperature variations drive phase transformations. The inclusion of nanoparticles enhances thermal conductivity, leading to a faster phase change process and improved heat transfer efficiency, thereby optimizing the thermal energy storage and release mechanism in heat exchanger applications.

In numerical simulations, enthalpy is integrated into the energy conservation equation, influencing the heat transfer dynamics during melting and solidification. By expressing enthalpy as a temperature-dependent function, the phase transition process can be accurately modeled, ensuring better thermal performance predictions for nanoPCM-based systems.

This method aids in tracking the heat absorption and release during both the charging and discharging phases. Enthalpy increases as heat is absorbed, indicating the phase change from solid to liquid, while it decreases during solidification as thermal energy is released. Monitoring these changes provides crucial insights into the system's thermal behavior, enabling better optimization of heat exchanger designs that utilize nanoPCM for enhanced energy management.

By integrating this into numerical simulations, the study thoroughly examines the melting behavior and thermal performance of nanoPCM in U-tube heat exchangers, supporting the development of high-efficiency thermal storage systems that can operate effectively across varying temperature ranges and phase transitions [10].

For this research, $CaCl_6H_2O$ was chosen as the primary PCM because of its advantageous thermal energy storage characteristics, including a high latent heat and a suitable temperature for phase transition. However, its inherently low thermal conductivity poses a challenge in applications requiring rapid heat transfer. To address this issue and improve the thermal response of the PCM, Al_2O_3 nanoparticles were introduced into the material. The nanoparticles were considered to be uniformly distributed within the PCM matrix at volume fractions of 1% and 2%, aiming to enhance thermal conductivity without significantly altering the latent heat storage capacity. Among various candidate

nanomaterials, Aluminum oxide (Al_2O_3) was specifically chosen for several compelling reasons: (1) it offers significantly higher thermal conductivity (~30 W/m·K) compared to the base PCM, (2) it is chemically stable and does not react with the salt hydrate PCM, (3) it is widely available and cost-effective, making it a practical choice for potential large-scale applications. This research examines how the distribution and concentration of these nanoparticles impact the thermal performance.

Incorporating Al_2O_3 nanoparticles into the PCM improves its thermal conductivity by creating pathways that facilitate heat transfer. Al_2O_3 was chosen due to its excellent thermal conductivity, stability, and suitability for high-temperature applications, making it a great addition to enhance PCM performance. This research examines how the distribution and concentration of nanoparticles impact the thermal properties of the nanoPCM, particularly how different Al_2O_3 volume fractions affect heat transfer efficiency and phase transition behavior.

To compute the effective thermal conductivity of the nanoPCM, the following equation is used [11]:

$$k_{nanoPCM} = k_{PCM}\left(1 + \phi\left(\frac{k_p - k_{PCM}}{k_p + 2k_{PCM}}\right)\right) \tag{5}$$

Here, $k_{nanoPCM}$ denotes the effective thermal conductivity of the nanoPCM, while k_{PCM} refers to the thermal conductivity of the base PCM ($CaCl_6H_2O$). Similarly, kp represents the thermal conductivity of the nanoparticles (Al_2O_3), and ϕ indicates the volume fraction of the nanoparticles.

For the calculation of other thermophysical properties of the nanoPCM, such as density, specific heat capacity, and viscosity, the widely accepted classical mixture models are employed [12], as shown in Equations (6)–(8). These models are selected for their robustness and common use in macroscopic thermal analysis, providing a foundational understanding of the bulk property changes. It is acknowledged that these models do not account for nanoparticle agglomeration or the temperature dependency of properties, which can be subjects of more detailed future investigations. These properties are crucial for the precise simulation of heat transfer and phase change behavior within the system.

Accurately determining the thermal conductivity of nanoPCM is crucial for assessing its enhanced heat transfer capabilities, which directly influence the efficiency of phase transitions and thermal management within the heat exchanger. By improving thermal conductivity, the phase change process is expedited, increasing heat transfer during both charging and discharging cycles, thereby enhancing the efficiency of energy storage and release.

Tables 1 and 2 provide the essential thermophysical properties of $CaCl_6H_2O$ and Al_2O_3 nanoparticles, which are key to modeling and simulating the nanoPCM's thermal behavior under various conditions. Incorporating these properties into the numerical analysis helps optimize the design of thermal energy storage systems that use nano-enhanced PCMs, ultimately enhancing the performance of shell-and-tube heat exchangers in energy storage applications.

Additional thermophysical properties of the nanoPCM, including density, specific heat capacity, and viscosity, were determined using the established mixture models presented in Equations (6)–(8) [12]. These properties are crucial for precise simulations of heat transfer and phase change behavior within the system.

Equation (6) determines the density of nanoPCM by considering the characteristics of both the base PCM and the embedded nanoparticles. Since density influences fluid flow characteristics within the heat exchanger, an accurate estimation that accounts for the mass contributions of both components is essential for modeling thermal performance.

$$\rho_{nanoPCM} = (1 - \phi)\rho_{PCM} + \phi\rho_p \tag{6}$$

where $\rho_{nanoPCM}$ is the density of the nanoPCM, ρ_{PCM} is the density of the base PCM ($CaCl_6H_2O$), ρp is the density of the nanoparticles (Al_2O_3), and ϕ is the volume fraction of nanoparticles.

Equation (7) is applied to determine the specific heat capacity of the nanoPCM, which is vital for evaluating its thermal energy storage and release capabilities during phase transitions. The effective

specific heat capacity is calculated by considering the contributions from both the base PCM and the nanoparticles. This property is crucial for determining the overall energy storage efficiency of the system and optimizing its thermal performance.

$$C_{p,nanoPCM} = (1-\phi)C_{p,PCM} + \phi C_{p,p} \tag{7}$$

Here, $C_{p,nanoPCM}$ represents the specific heat capacity of the nanoPCM, while $Cp_{,PCM}$ and $C_{p,p}$ correspond to the specific heat capacities of the base PCM and the nanoparticles, respectively.

Finally, Equation (8) is applied to calculate the viscosity of the nanoPCM, a crucial factor for assessing the fluid flow behavior inside the heat exchanger. Viscosity plays a vital role in convective heat transfer and directly impacts the thermal efficiency of the system. The effective viscosity of the nanoPCM is determined through a modified formula that incorporates the influence of the dispersed nanoparticles, reflecting their effect on the flow characteristics and overall performance of the heat exchanger.

$$\mu_{nanoPCM} = \mu_{PCM}\left(1 + \phi \cdot \left(\frac{\mu_p - \mu_{PCM}}{\mu_p + 2\mu_{PCM}}\right)\right) \tag{8}$$

In this expression, $\mu_{nanoPCM}$ denotes the viscosity of the nanoPCM, μ_{PCM} represents the viscosity of the base PCM, μ_p corresponds to the viscosity of the nanoparticles, and ϕ indicates the volume fraction of the nanoparticles.

By determining these essential properties, the study enables a thorough analysis of the nanoPCM's behavior within the U-tube heat exchanger system. These characteristics are critical for modeling heat transfer, forecasting the phase change dynamics, and refining the design and efficiency of nano-enhanced PCM-based thermal energy storage systems. Gaining insights into how nanoparticles alter the thermophysical properties of the PCM contributes to a more precise and comprehensive assessment of the potential advantages for practical applications.

Table 1. Thermophysical properties of $CaCl_26H_2O$ [13]

Thermophysical properties	**$CaCl_26H_2O$**
Melting point	29.6°C
Latent heat of fusion	190.8 kJ/kg
Specific heat capacity (liquid)	2.10 kJ/kgK
Specific heat capacity (solid)	1.42 kJ/kgK
Density (liquid)	1.562×10^3 kg/m³
Density (solid)	1.802×10^3 kg/m³
Thermal conductivity (liquid)	0.540 W/mK
Thermal conductivity (solid)	1.088 W/mK
Viscosity	0.0118 kg/ms
Molar mass	219.0784 g/mol

Table 2. Thermophysical properties of Aluminum oxide [14]

	ρ (kg/m³)	**k (W/m.K)**	**c_p (J/ kg.K)**
(Al_2O_3)	3600	30	880

2.2. Initial and Boundary Conditions

The accuracy of the numerical simulation is critically dependent on the precise definition of the initial and boundary conditions, which were established to replicate the experimental setup described in the validation study [15].

Initial Conditions:

At the start of the melting process (t=0), the entire PCM domain was assumed to be in a uniform solid state. The initial temperature was set to Tinitial = 29.0 °C, a value just below the melting point of

$CaCl_2 \cdot 6H_2O$ (29.6 °C) to ensure no liquid phase was present initially. The fluid inside the tubes was also assumed to be stationary at this temperature.

Boundary Conditions:

The boundary conditions applied to the computational domain are defined as follows:

- Hot Fluid Inlet: Hot water was introduced into the U-tube inlet with a constant temperature of Tinlet = 60 °C and a uniform velocity profile corresponding to a flow rate of 10 L/min, which calculates to an average velocity of Vinlet = 0.83 m/s. These values were chosen to provide a sufficient temperature gradient to drive the phase change process effectively.
- Tube Walls: A no-slip boundary condition (u=0) was applied to the inner surfaces of the U-tube walls. For the thermal condition, a coupled wall interface was defined between the fluid, the tube walls, and the PCM. This ensures that the heat flux and temperature are continuous across the material interfaces, allowing for accurate modeling of conjugate heat transfer.
- Fluid Outlet: A pressure-outlet boundary condition was set at the tube outlet, with a gauge pressure of 0 Pa. This condition assumes a fully developed flow at the exit.
- Outer Shell: The external wall of the heat exchanger shell was treated as adiabatic (perfectly insulated). This implies that there is no heat transfer between the system and the surroundings, so the heat flux across this boundary is zero ($\partial T/\partial n = 0$). This condition isolates the thermal process within the heat exchanger.

3. GRID INDEPENDENCE

To guarantee that the simulation outcomes were not influenced by the mesh density, a series of grid independence tests was meticulously performed. The grids were systematically generated using the commercial software ANSYS Meshing, with the spatial distribution of the grid visualized in Figure 2. To validate the accuracy of the simulation, various grid sizes and element counts were used, and the detailed outcomes of the grid independence test are presented in Figure 3. These tests were carefully performed to assess the influence of higher-resolution grids on the performance of the model and to confirm the reliability of the simulation results.

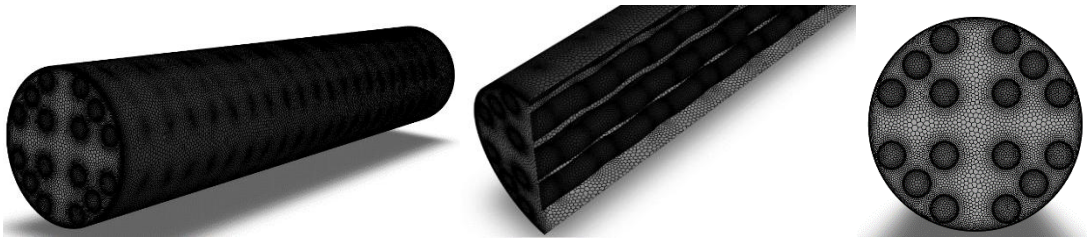

Figure 2. Grid distribution

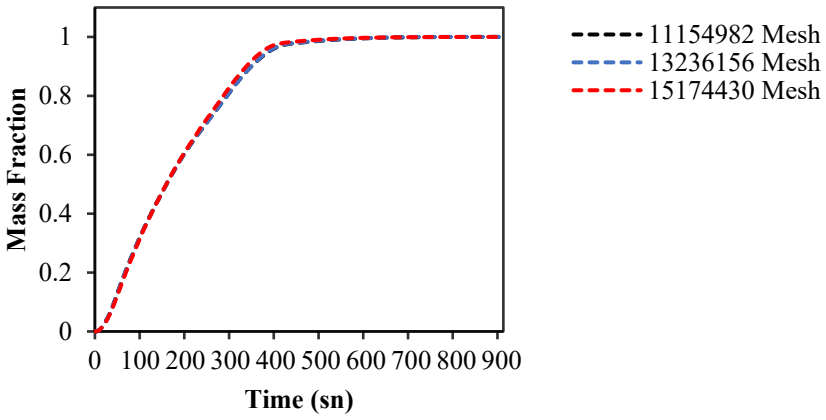

Figure 3. Grid independency

4. FINITE ELEMENT ANALYSIS OF THERMAL PERFORMANCE

This section presents a detailed numerical analysis of the thermal performance of a U-tube heat exchanger incorporating PCMs enhanced with Al2O3 nanoparticles. The use of numerical methods, such as Finite Element Analysis (FEA), is a well-established and reliable approach for investigating energy storage phenomena in PCMs, with studies like Berent et al. [4] demonstrating strong agreement between numerical and analytical models. Building on this foundation, a critical first step in our analysis was to validate our specific numerical model to ensure its accuracy. The model's predictions were rigorously compared against the experimental findings reported by Çakmak [15]. The validation case was specifically chosen to match the experimental setup: a straight-tube heat exchanger containing pure PCM (0% nanoparticles), subjected to the same initial and boundary conditions. Figure 4 presents a direct comparison of the liquid mass fraction evolution over time between the numerical simulation (solid line) and the experimental data points (markers). The results show an excellent agreement, with a mean absolute error of less than 4%, confirming that the developed finite element model can accurately capture the complex physics of the melting process. With the model's reliability established, the study was extended to investigate the effects of nanoparticle addition and wavy tube geometry.

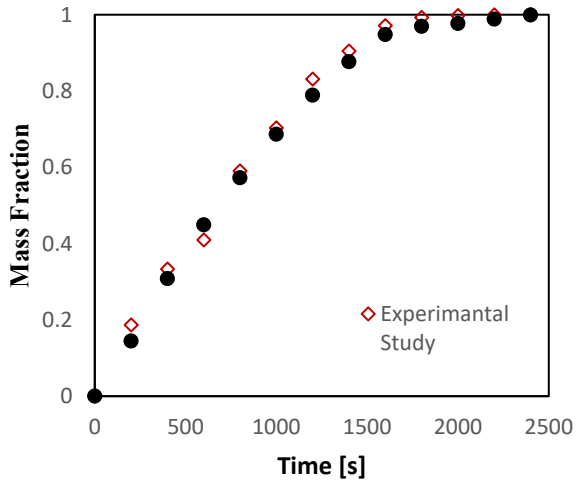

Figure 4. Validation of the numerical model: comparison of the simulated mass fraction evolution (solid line) against experimental data from çakmak [15] (markers) for the straight-tube configuration with pure pcm

Figure 4 illustrates this validation process, comparing the mass fraction evolution between our numerical study and the experimental results. The strong correlation between both datasets demonstrates the model's capability to predict the melting dynamics of PCMs. Subsequently, Figure 5 presents mass fraction contours within the U-tube heat exchanger with a straight tube, visually depicting the melting process from solid to liquid as heat is transferred from the working fluid. The complete phase transition of PCM was observed within 2503 seconds, confirming the expected thermal response of the system.

Following the validation phase, the study was extended to examine the effect of Al_2O_3 nanoparticle inclusion in the PCM at concentrations of 1% and 2%. The mass fraction contours shown in Figure 6 highlight the melting behavior of the nano-enhanced PCM under these conditions. The results revealed a significant reduction in phase change duration: the PCM with 1% Al_2O_3 nanoparticles melted within 600 seconds, while the PCM with 2% Al_2O_3 nanoparticles exhibited an even faster melting process, completing phase change within 480 seconds.

The mechanism behind this substantial improvement lies in the enhanced thermal conductivity of the composite, a direct result of the Al2O3 nanoparticle inclusion, which collectively establishes a more efficient pathway for heat transfer. The increased thermal diffusivity allowed heat to be distributed more uniformly, accelerating the melting rate and optimizing energy absorption. Notably, the use of a wavy

tube configuration further contributed to improved heat transfer performance, as it promoted better thermal distribution, especially in regions where conduction-dominated melting was prevalent.

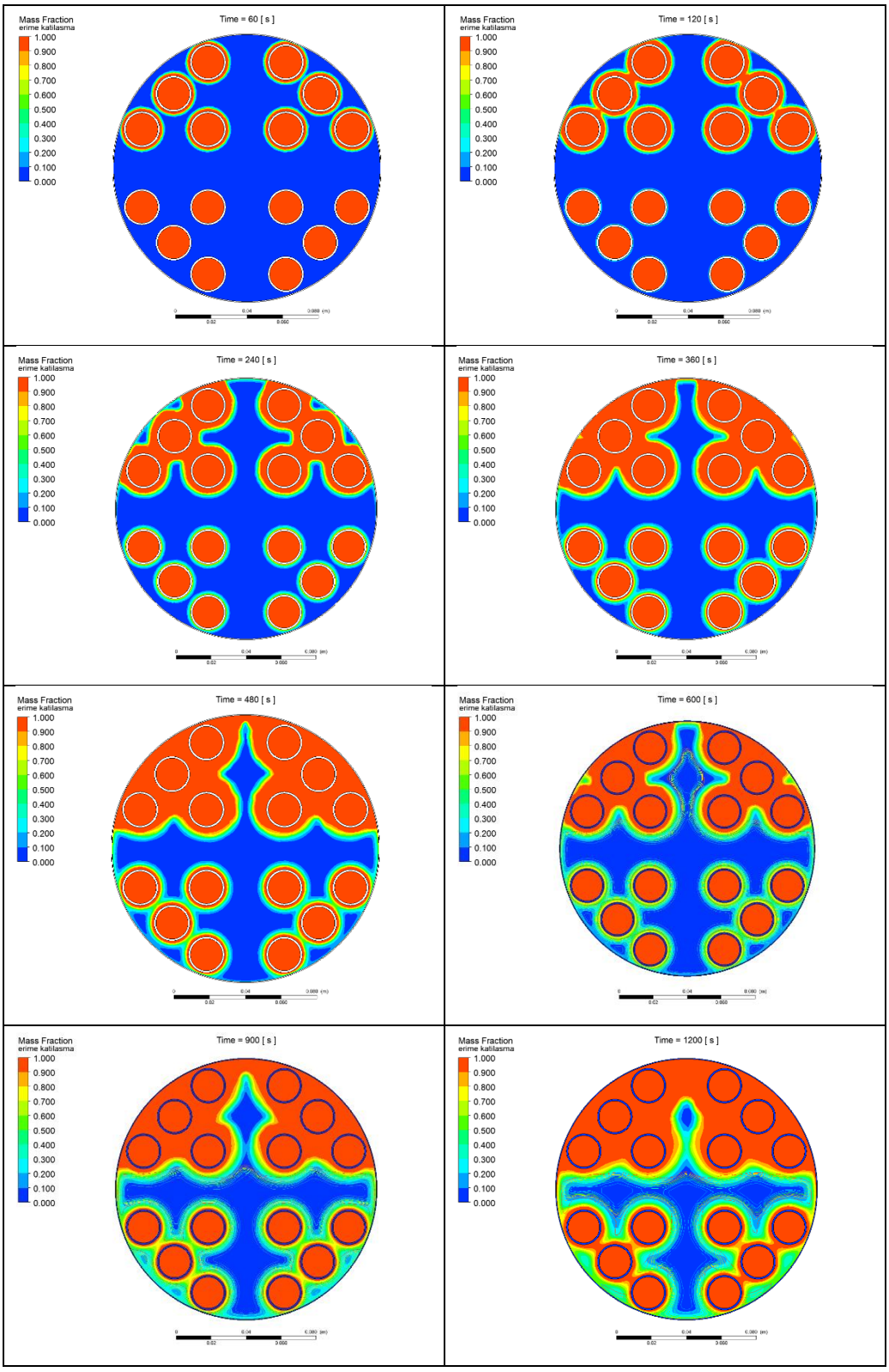

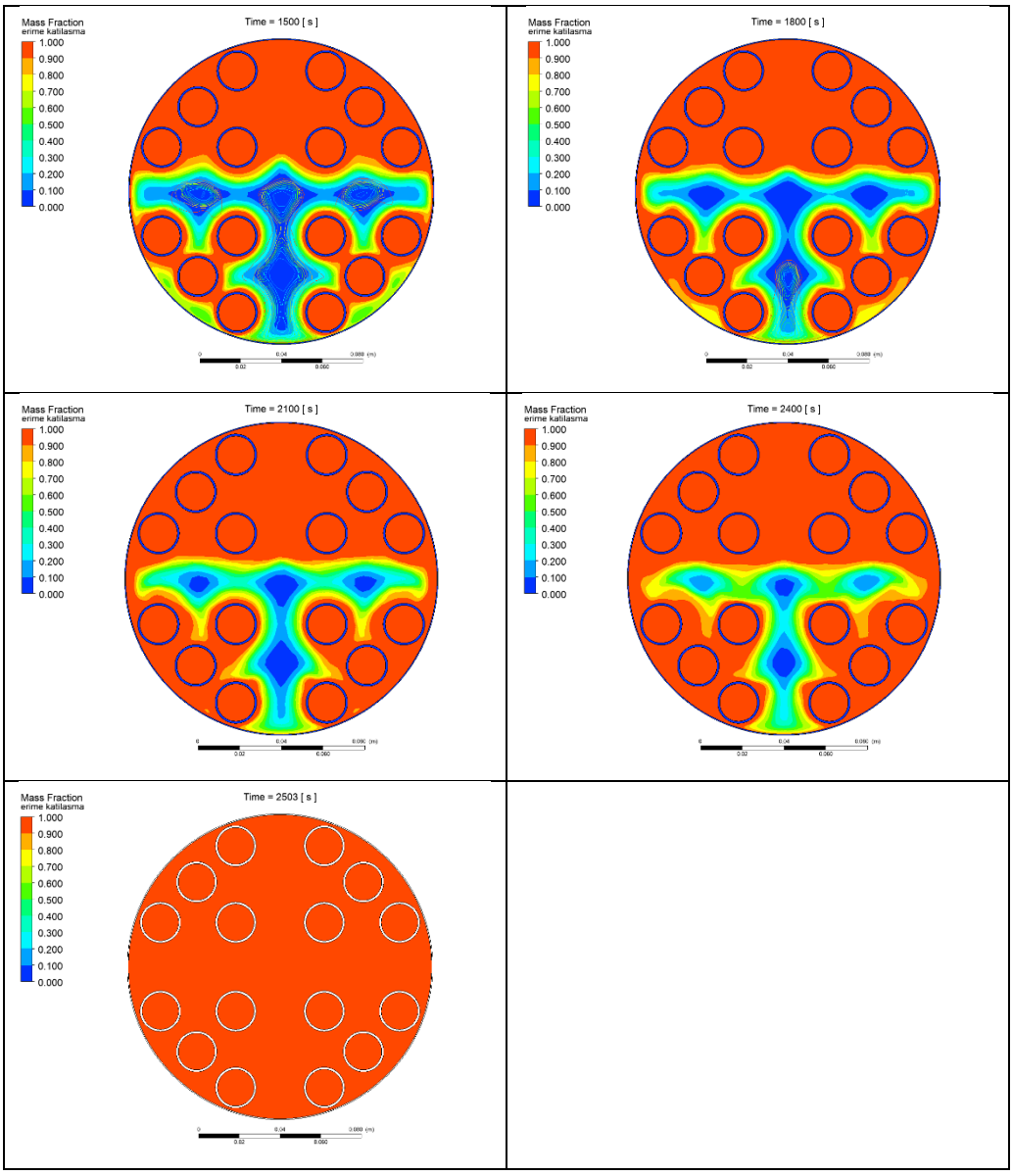

Figure 5. Mass fraction contours in a u-tube heat exchanger with straight tubes filled with pcm

Figure 7 provides a comparative analysis of the time-dependent mass fraction evolution for different configurations, demonstrating the impact of both the wavy tube structure and nano-enhanced PCM. The wavy tube's ability to induce secondary flow and disrupt thermal boundary layers played a key role in expediting the melting process. This structural flexibility ensured that heat was more uniformly distributed, preventing localized overheating and resulting in an overall enhancement of heat exchanger performance.

A quantitative analysis of these results reveals the individual and combined contributions of the wavy tube geometry and nanoparticle addition. For the baseline case with a straight tube and pure PCM (as shown in Fig. 5), the total melting time was 2503 s. Introducing the wavy tube geometry alone (with 0% nanoparticles) reduced the melting time to approximately 900 s (Fig. 7), a significant reduction of about 64% attributable to the enhancement of natural convection currents. The most dramatic improvement, however, was observed when both strategies were combined: the wavy tube with 2% nano-enhanced PCM completed melting in just 480 s, representing a total time reduction of nearly 81% compared to the baseline. This demonstrates a strong synergistic effect, where the wavy geometry promotes convective heat transfer while the nanoparticles boost thermal conduction, together accelerating the phase change process far more effectively than either method alone.

The findings from this study underscore the significant potential of nanoparticle-enhanced phase change materials in optimizing heat exchanger efficiency. The integration of 2% Al_2O_3 nanoparticles within the PCM resulted in the highest liquid fraction at the end of the melting cycle, demonstrating superior thermal energy storage capacity and improved phase change dynamics. The accelerated heat transfer, facilitated by both the nanoparticles and the wavy tube design, led to a more responsive and efficient thermal management system.

Wavy tube filled with PCM with 0% Al_2O_3	Wavy tube filled with PCM with 1% Al_2O_3	Wavy tube filled with PCM with 2% Al_2O_3
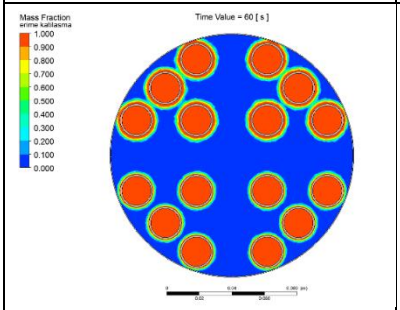	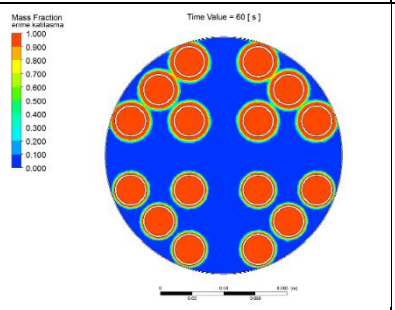	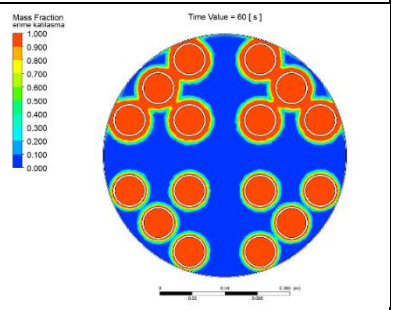
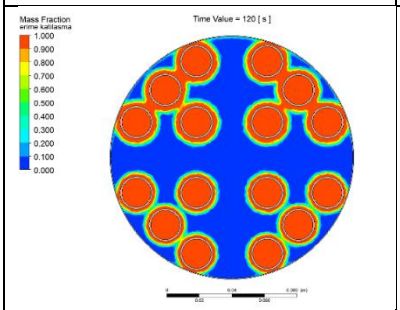	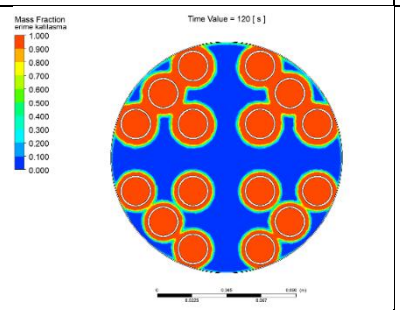	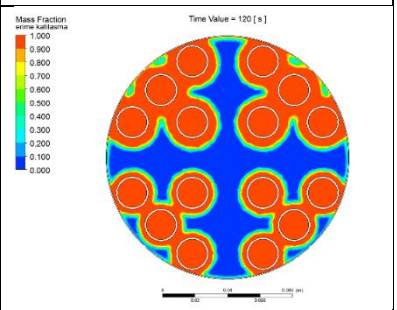
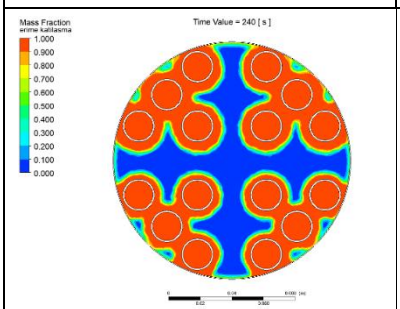	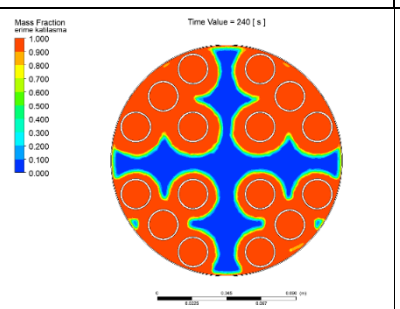	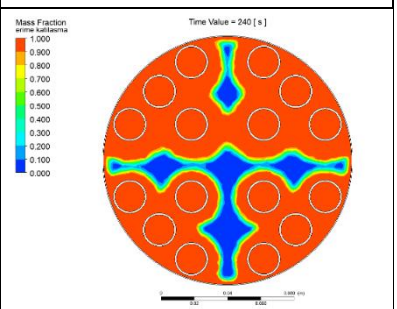
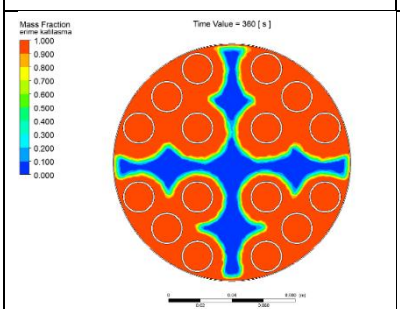	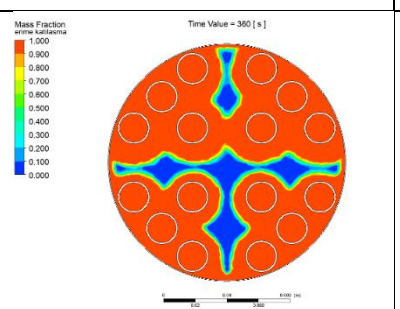	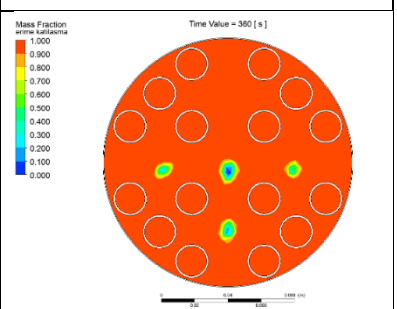

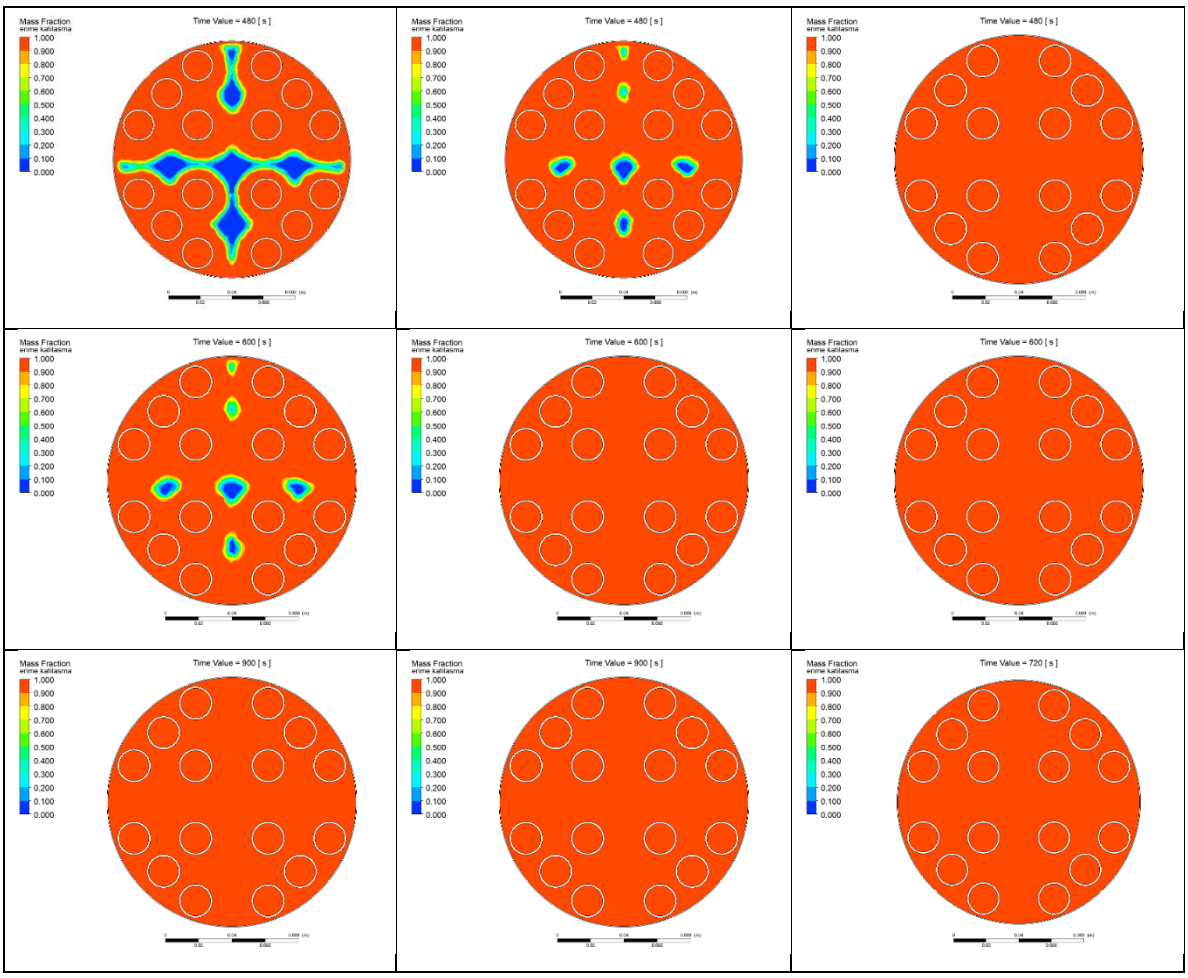

Figure 6. Mass fraction contours in a u-tube heat exchanger with wavy tube

By combining advanced nanomaterial modifications with innovative geometric configurations, this study highlights a promising pathway for enhancing heat exchanger performance in energy storage applications. The improved heat absorption and phase change efficiency offered by nanoPCM-based heat exchangers can contribute to more effective energy utilization in thermal management systems, making them particularly relevant for applications in renewable energy storage, industrial waste heat recovery, and sustainable engineering solutions.

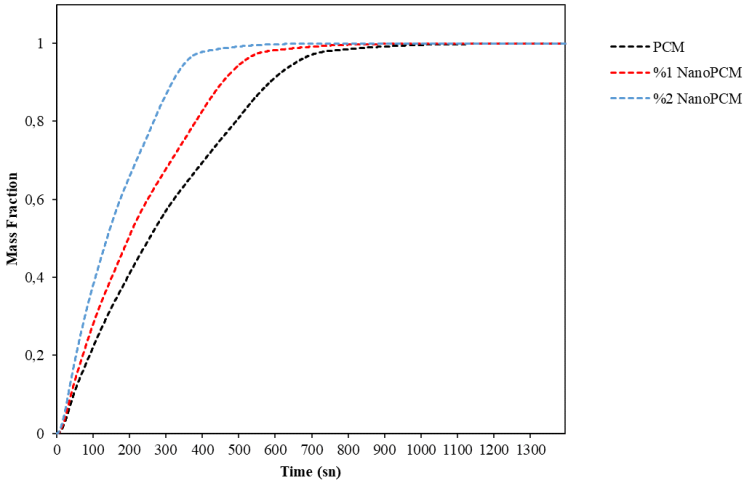

Figure 7. Time-dependent mass fraction

In conclusion, this study provides valuable insights into the integration of nanotechnology with novel heat exchanger designs, paving the way for further research and technological advancements in phase change-based thermal energy storage. Future work could explore the impact of different nanoparticle materials, alternative tube geometries, and experimental validation to further refine and optimize heat exchanger performance for large-scale applications.

5. ANFIS-BASED PREDICTION AND OPTIMIZATION OF MELTING PROCESS

While FEA provides a detailed and accurate method for simulating the complex thermal dynamics in the PCM-integrated heat exchanger, it has a significant limitation: high computational cost. Performing extensive parametric studies or optimization analyses, which require evaluating numerous combinations of variables like nanoparticle concentration (ϕ), time (t), and pipe geometry, becomes prohibitively expensive in terms of time and resources.

This study introduces an ANFIS-based surrogate model as a solution to this challenge, enabling both rapid prediction and effective optimization of the system's thermal performance without the computational overhead of traditional methods. ANFIS stands out as a powerful hybrid intelligent system by integrating the adaptive learning mechanisms of neural networks with the transparent, rule-based reasoning of fuzzy logic [16].

Using a dataset generated via FEA, the ANFIS model was trained to map the complex, non-linear relationship between the system's input variables (time, concentration, pipe type) and its primary output, the liquid mass fraction. This provides it with the ability to make instantaneous and highly accurate predictions without the need to run time-consuming FEA simulations for each new condition. The primary goal of this section is to validate the developed ANFIS model and then use this rapid model to perform an optimization analysis to determine the optimal nanoparticle concentration that minimizes the total melting time.

5.1. Dataset Generation and ANFIS Architecture

The dataset required for training and testing the ANFIS model was generated using the FEA model described in the previous sections of this study. To represent the model's performance over a wide operational range, numerous simulations were systematically performed for different input parameters.

The input and output variables for the developed ANFIS model are defined as follows:

Input Variables:

Time (t): Represents the time in the melting process (s).

Nanoparticle Concentration (ϕ): Represents the volume percentage of Al2O3 nanoparticles in the PCM (%).

Pipe Geometry: A categorical variable indicating the pipe geometry used in the heat exchanger (0 = Straight Pipe, 1 = Wavy Pipe).

Output Variable:

Liquid Mass Fraction: A dimensionless value between 0 (fully solid) and 1 (fully liquid) that indicates how much of the PCM has transitioned to the liquid phase at a given moment.

In this context, a dataset consisting of 97 different simulation scenarios was generated. To improve the performance of the ANFIS model and prevent inputs with different scales from disproportionately influencing the model, all input data were normalized to the [0, 1] range.

ANFIS Architecture and Training

In this study, a Sugeno-type ANFIS model was used. The model's architecture consists of five layers: (1) Fuzzification, (2) Rule, (3) Normalization, (4) Defuzzification, and (5) Total Output. This architecture is schematically shown in Figure 8.

Each layer of the model performs a specific mathematical function:

Layer 1 (Fuzzification Layer): The first layer in the ANFIS architecture is the Fuzzification Layer, which functions to transform the crisp numerical inputs into linguistic fuzzy sets through membership functions. This is accomplished through predefined membership functions (MFs) for each input. In this study, the generalized bell-shaped membership function ('gbellmf') was used. The output of the i-th membership function for an input x is calculated as:

$$\mu A_i(x) = 1 / (1 + |(x - c_i)/a_i|^{2b_i}) \quad (9)$$

where a_i, b_i and c_i, are the premise parameters that the model learns during training, defining the shape (width, slope, and center) of the membership function.

Layer 2 (Rule Layer): The function of the second layer (Rule Layer) is to evaluate the firing strength (wi) of each potential IF-THEN rule. This is accomplished by multiplying the membership degrees for the respective inputs at each node. The output of the i-th rule is:

$$w_i = \mu\_t(t) \times \mu\_\phi(\phi) \times \mu\_ \text{Pipe(Pipe Geometry)} \quad (10)$$

Layer 3 (Normalization Layer): In the third layer, known as the Normalization Layer, the firing strength of each rule is scaled by calculating its ratio to the total firing strength of all rules. This determines the relative contribution of each rule to the total output. The normalized firing strength ($\bar{w}_i$) is:

$$\bar{w}_i = w_i / (\Sigma w_j) \quad (11)$$

Layer 4 (Defuzzification Layer): Each node in this layer multiplies the normalized firing strength by a function of the consequent part of the rule. In a Sugeno-type model, this is a linear combination of the inputs:

$$O^4_i = \bar{w}_i * f_i = \bar{w}_i * (p_i t + q_i \phi + r_i \text{ Pipe} + s_i) \quad (12)$$

where p_i, q_i, r_i and s_i, are the consequent parameters determined during the training process.

Layer 5 (Total Output Layer): The final stage of the ANFIS process occurs in Layer 5, where a single summation node aggregates the outputs from the defuzzification layer to produce the final, crisp prediction for the Liquid Mass Fraction.

$$f = \Sigma \bar{w}_i * f_i = (\Sigma w_i * f_i) / (\Sigma w_i) \quad (13)$$

This layered structure allows ANFIS to model complex non-linear relationships with high accuracy.

The training process for the model was configured with the following parameters:

Data Splitting: The generated 97-point dataset was randomly divided into two sets to test the model's generalization ability. Approximately 70% of the data (68 data points) was used for training the model, while the remaining 30% (29 data points) was used for testing its performance on unseen data.

Membership Functions: Gaussian bell-shaped membership functions ('gbellmf') were chosen for each input variable. 4, 3, and 2 membership functions were defined for the time, concentration, and pipe type inputs, respectively. This selection aims to effectively partition the input feature space.

Training Algorithm and Duration: The ANFIS model was trained using the standard hybrid learning algorithm, which combines gradient descent and least squares estimation methods. The training was conducted for a total of 150 epochs.

After the training process was completed, the final state of the learned membership functions for each input variable was visualized. Figure 9 illustrates how the ANFIS model partitioned and interpreted the

input space. For example, in the "Input 2 (Concentration %)" graph, the membership functions are denser and more overlapping in specific regions of the data range (e.g., 0.2-0.6 range), indicating that the model is more sensitive to data changes in these regions and has learned more detailed fuzzy rules.

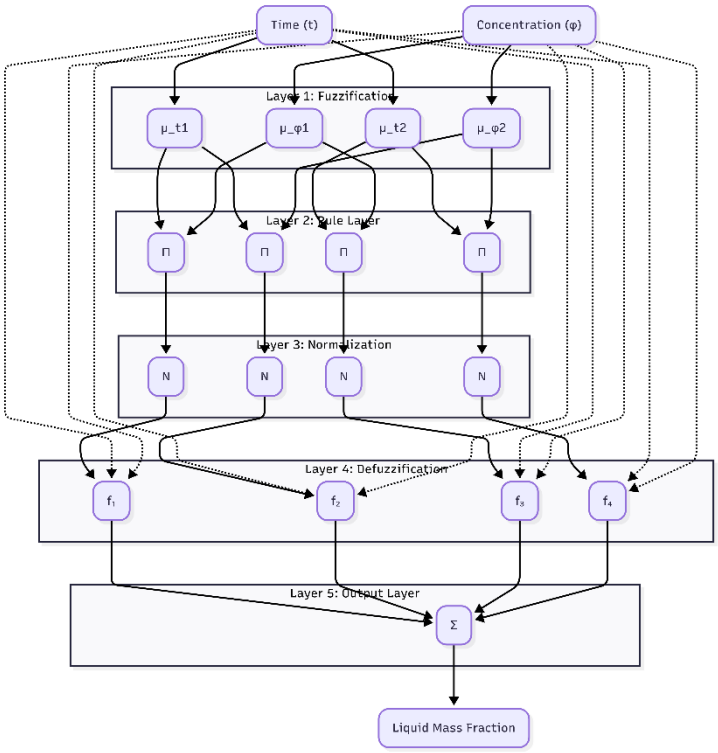

Figure 8. The general five-layer ANFIS architecture. For visual clarity, the diagram is simplified to show two inputs (Time and Concentration), while the full model utilizes three inputs (Time, Concentration, and Pipe Geometry)

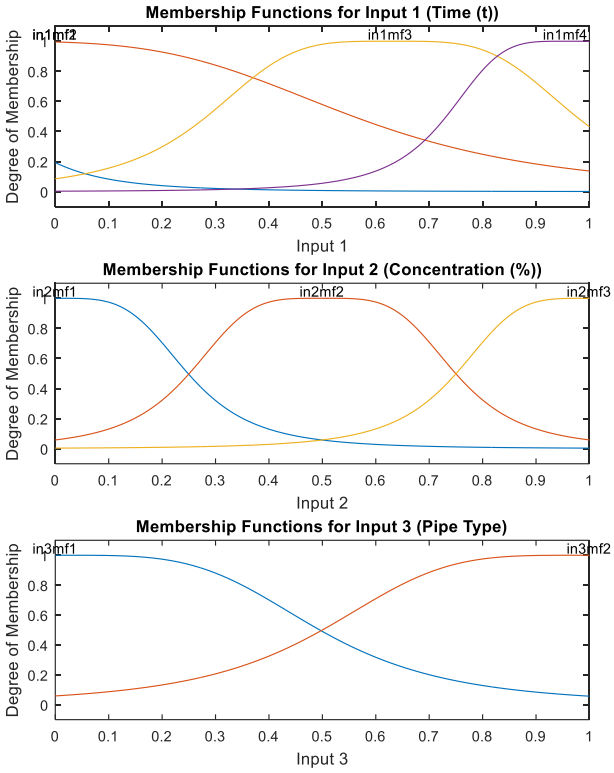

Figure 9. Membership functions for each input variable after the ANFIS training process

5.2. Model Validation and Performance

To assess the reliability and prediction accuracy of the ANFIS model, a validation analysis was performed on the independent test dataset. The model's performance was evaluated using both quantitative error metrics and visual comparisons.

The training process of the model is presented in Figure 10. In this graph, it is observed that the Root Mean Square Error (RMSE) of the model rapidly decreases as the training epochs progress and converges to a stable value after the first few epochs. This indicates that the model successfully captured the underlying relationships in the dataset without overfitting.

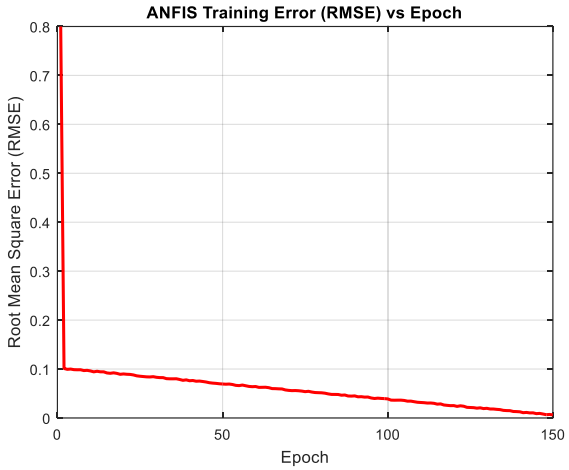

Figure 10. ANFIS training error (rmse) vs epoch

The model's true success is measured by its generalization ability, which was evaluated on the test dataset. In Figure 11, the values predicted by the ANFIS model are compared against the actual values obtained from FEA in a scatter plot.

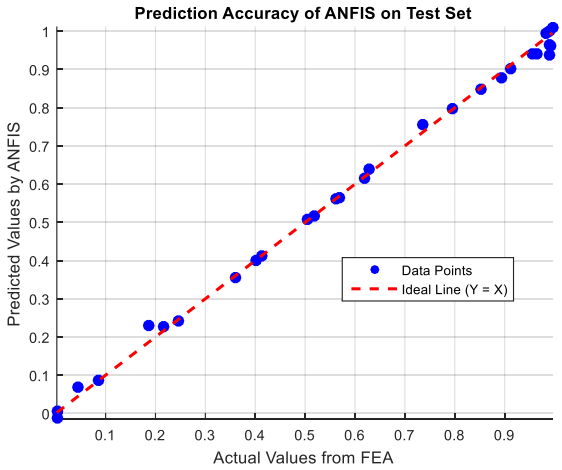

Figure 11. Prediction accuracy of anfis on test set

The tight clustering of data points around the Y=X line, which represents a perfect match, indicates that the model has high prediction accuracy. To quantify this visual agreement, the performance metrics calculated on the test dataset are summarized in Table 3.

As seen in the table, the error metrics (RMSE and MAE) are extremely low for both datasets. The small difference between the training error (RMSE = 0.008160) and the test error (RMSE = 0.017521)

demonstrates that the model avoided overfitting and can successfully generalize its learned knowledge to new, unseen data.

Table 3. Performance metrics of the ANFIS model on different datasets

Data Type	Root Mean Square Error (RMSE)	Mean Absolute Error (MAE)	R-Square (R^2)
Training Data	0.008160	0.006532	-
Test Data	0.017521	0.012423	0.997345

Furthermore, the R^2 value of 0.9973 calculated for the test set reveals that the model can explain over 99.7% of the variability in the FEA simulation results. This high R-square value and the low error metrics strongly confirm that the developed ANFIS model can reproduce the FEA results with high fidelity and is therefore a reliable surrogate model for optimization studies (Figure 12).

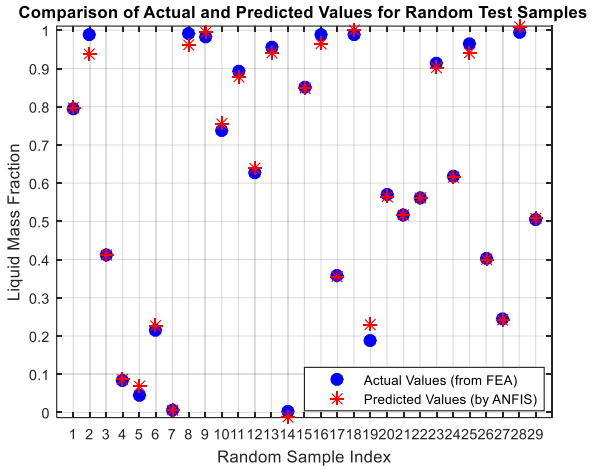

Figure 12. Comparison of actual and predicted values for random test samples

5.3. Optimization of Nanoparticle Concentration

Beyond being just a prediction tool, the trained and validated ANFIS model was used as a powerful and fast tool to optimize the system's thermal performance. In this section, an optimization analysis was performed using the ANFIS surrogate model to determine the optimal nanoparticle concentration (ϕ) that minimizes the melting time, without needing to run FEA simulations that could take hours for each scenario.

The optimization was performed for the wavy pipe geometry (Pipe Geometry = 1), which is known to exhibit the best thermal performance. In the analysis, the nanoparticle concentration was varied between 0% and 10%, and for each concentration value, the minimum time required for the complete melting of the PCM (liquid mass fraction ≈ 1) was calculated in seconds using an optimization algorithm (fminbnd) on the ANFIS model. The results of the optimization analysis are presented in Figure 13.

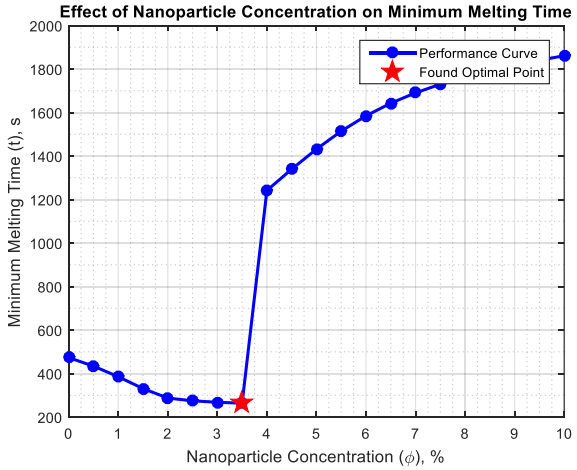

Figure 13. Effect of nanoparticle concentration on minimum melting time

This graph clearly shows the effect of nanoparticle concentration on the minimum melting time. As seen in the graph:

Compared to pure PCM (0% concentration), the addition of small amounts of nanoparticles significantly reduces the melting time by increasing the thermal conductivity of the PCM.

The melting time reduction becomes more pronounced with increasing nanoparticle content, ultimately reaching an optimal minimum at a concentration of approximately 3.5%.

However, after exceeding a concentration of 3.5%, the melting time begins to increase again. This can be explained by negative effects, such as the increase in the nanofluid's viscosity at high concentrations, starting to dominate over the positive gain in thermal conductivity. This increased viscosity slows down the natural convection currents, thus reducing the heat transfer efficiency.

The analysis concluded that the optimal performance for the system is achieved at a nanoparticle concentration of 3.50%. At this optimal concentration, the predicted minimum melting time was calculated as 263.63 seconds. This result establishes a critical design parameter, enabling performance maximization while mitigating material costs in the development of thermal energy storage systems.

5.4. Discussion on the ANFIS Model Robustness and Generalization

The robustness of the developed ANFIS model is inherently tied to the training data generated by the FEA simulations. Since the thermophysical properties, including nanoparticle-enhanced viscosity, were defined by established correlations (Eq. 5-8) within the FEA model, the ANFIS model has learned the system's behavior based on these specific formulations. Significant deviations in real-world thermophysical properties from these correlations—for instance, due to nanoparticle agglomeration affecting viscosity more than predicted—would likely reduce the model's accuracy. Therefore, the current model is robust within the physical framework defined by the FEA. For applications with different nanoparticles or base fluids, where property correlations might differ, it is recommended to either retrain the model with new FEA data or incorporate property variations as an additional input parameter to enhance its robustness.

The generalization capability of the ANFIS model is directly influenced by the size and diversity of the training dataset. The 97-point dataset used in this study was strategically generated to cover the key design space for the specified PCM and nanoparticle type, resulting in a high accuracy ($R^2 > 0.997$). Increasing the dataset size, particularly by including more data points in regions of high nonlinearity (such as around the optimal concentration), could further enhance the model's generalization and potentially capture more subtle physical effects. However, the current ANFIS framework is specific to the $CaCl_2 \cdot 6H_2O$-Al_2O_3 system. Due to the unique thermophysical properties (e.g., melting point, latent heat, viscosity) of different PCMs or nanoparticles, the model cannot be directly reused for another material system. Each new system would require generating a new dataset via FEA and completely

retraining the ANFIS model. Nevertheless, the methodology itself—the hybrid FEA-ANFIS approach—is highly generalizable and serves as a template for optimizing a wide range of thermal systems.

Scaling this hybrid approach to large-scale, real-world energy storage applications presents both challenges and opportunities. Direct FEA simulation of a full-scale system would be computationally prohibitive. However, the methodology can be adapted in several ways. First, simplified or dimensionally-reduced FEA models (e.g., porous media approximations) could be used to generate the training data, reducing the computational burden while still capturing the dominant physics. Second, the ANFIS model, once trained, can be integrated into larger system-level simulation tools (e.g., MATLAB Simulink, TRNSYS) to represent the thermal storage unit's dynamic behavior without the need for co-simulation with heavy FEA software. Finally, for real-world deployment, the surrogate model could be further refined with operational data, bridging the gap between numerical predictions and actual performance. This would enable real-time optimization and control of large thermal energy storage systems, highlighting the practical potential of this hybrid intelligence approach beyond the design phase.

6. CONCLUSIONS

This study has successfully demonstrated a high-performance framework for thermal energy storage by synergizing nanotechnology, advanced wavy geometries, and artificial intelligence. The hybrid FEA-ANFIS approach effectively addressed the computational bottlenecks associated with traditional design methods. The key findings are highlighted as follows:

1. Synergistic Thermal Enhancement: The integration of Al_2O_3 nanoparticles and wavy tube geometry resulted in a remarkable 81% reduction in melting time compared to the baseline straight-tube design. While the wavy tubes accelerate melting by promoting natural convection currents, the nanoparticles significantly boost the effective thermal conductivity of the PCM.
2. AI-Driven Design Precision: The developed ANFIS surrogate model achieved exceptional predictive accuracy with an $R^2 > 0.997$. This model enables the optimization process to be completed in seconds rather than the hours required for intensive FEA simulations, proving to be a robust tool for rapid thermal management analysis.
3. The Critical Threshold (3.50%): Optimization analysis identified 3.50% as the ideal nanoparticle concentration, achieving a minimum melting time of 263.63 seconds. Beyond this threshold, the negative impact of increased viscosity begins to dominate over the gains in thermal conductivity, illustrating a vital design trade-off.

Future work should focus on experimentally validating the performance of the optimized nano-enhanced PCM in the wavy tube configuration. Furthermore, investigating the long-term stability and cycling performance of the nanoPCM, as well as exploring the effects of different nanoparticle types (e.g., copper oxide, graphene) and base PCMs, could yield further performance improvements. Finally, extending the hybrid model to include solidification (discharging) cycles would provide a more complete understanding of the entire thermal energy storage process.

Acknowledgements

This research received no specific grant from any funding agency in the public, commercial, or not-for-profit sectors.

Conflict of Interest Statement

The authors declare that they have no conflict of interest.

Statement of Research and Publication Ethics

The study complies with research and publication ethics. This study is based on numerical simulations and does not involve human participants or animals; therefore, formal ethics committee approval was not required.

Artificial Intelligence (AI) Contribution Statement

AI tools were used solely for linguistic polishing and grammatical corrections. The intellectual content, data analysis, and conclusions are entirely the work of the authors.

Contributions of the Authors

All authors contributed to the study conception and design. The numerical simulation and finite element analysis (FEA) were performed by Ali Taşkıran. The Adaptive Network-Based Fuzzy Inference System (ANFIS) modeling and optimization analysis were conducted by Taha Kubilay Şener. The overall conceptualization, validation, analysis of the results, and writing of the original manuscript were carried out by Gülşah Çakmak. All authors have read and approved the final manuscript.

REFERENCES

[1] J. Buongiorno et al., "Correct interpretation of nanofluid convective heat transfer," Int. J. Therm. Sci., vol. 129, pp. 504–531, 2018, doi: 10.1016/j.ijthermalsci.2017.07.002.

[2] M. Fadaei, M. Izadi, E. Assareh, and A. Ershadi, "Numerical modeling and optimization of a heat exchanger with integrated phase change materials," Appl. Therm. Eng., vol. 220, p. 119795, 2023, doi: 10.1016/j.applthermaleng.2022.119795.

[3] Q. Su et al., "Experimental and numerical investigation on the melting behavior of paraffin in a shell and tube latent heat storage unit," Appl. Therm. Eng., vol. 236, p. 121374, 2024, doi: 10.1016/j.applthermaleng.2023.121374.

[4] H. K. Berent, E. Cihan, and H. Demir, "Analytical and numerical comparison of the two-dimensional one- and two-phase energy storage phenomenon in phase change materials," Arab. J. Sci. Eng., 2025, doi: 10.1007/s13369-025-09998-8.

[5] F. M. Alharthi et al., "Finite element modeling of GFRP bar-reinforced hollow-core concrete beams under flexural loads," Arab. J. Sci. Eng., 2025, doi: 10.1007/s13369-025-10004-4.

[6] G. Xie et al., "Numerical and experimental investigations on the thermal-hydraulic performance of heat exchangers with Schwarz-P and gyroid structures," Int. J. Therm. Sci., vol. 197, p. 108748, 2024.

[7] J.-S. R. Jang, "ANFIS: Adaptive-network-based fuzzy inference system," IEEE Trans. Syst. Man Cybern., vol. 23, no. 3, pp. 665–685, 1993, doi: 10.1109/21.256541.

[8] Y. A. Çengel and A. J. Ghajar, Heat and Mass Transfer: Fundamentals and Applications, 6th ed. New York: McGraw-Hill Education, 2020.

[9] Y. M. El Hasadi and J. M. Khodadadi, "One-dimensional Stefan problem formulation for solidification of nanostructure-enhanced phase change materials (NePCM)," Int. J. Heat Mass Tran., vol. 67, pp. 202–213, 2013, doi: 10.1016/j.ijheatmasstransfer.2013.08.013.

[10] H. Ma and Y. Zhang, "Stochastic response analysis of 3D vibro-acoustic systems with geometrical uncertainties based on the extended finite element method," Int. J. Numer. Methods Eng., vol. 125, p. e7382, 2024, doi: 10.1002/nme.7382.

[11] Y. Cang, Y. Hu, L. Wang, and Y. Shen, "Numerical scheme solving the temperature of the interface between gas and heterogeneous solid with phase change," Int. J. Numer. Methods Eng., vol. 123, pp. 1036–1056, 2022, doi: 10.1002/nme.6887.

[12] Ansys Inc., ANSYS FLUENT Theory Guide, Release 20. ANSYS Inc., 2020. [Online]. Available: http://www.afs.enea.it/project/neptunius/docs/fluent/html/th/main_pre.htm

[13] M. Gür, H. F. Öztop, and F. Selimefendigil, "Numerical investigation of natural convection in a square cavity with a heat-generating porous medium and a circular cylinder," Renew. Energy, vol. 218, p. 119265, 2023, doi: 10.1016/j.renene.2023.05.118.

[14] W. Yu and S. U. S. Choi, "The role of interfacial layers in the enhanced thermal conductivity of nanofluids: A renovated Hamilton-Crosser model," J. Nanoparticle Res., vol. 6, pp. 355–361, 2004, doi: 10.1007/s11051-004-2601-7.

[15] G. Çakmak, "Experimental investigation of thermal storage in U-tube heat exchanger," Int. Commun. Heat Mass Tran., vol. 44, pp. 83–86, 2013, doi: 10.1016/j.icheatmasstransfer.2013.03.021.

[16] H. S. S. Aljibori et al., "An artificial intelligence–finite element study of magnetohydrodynamic heat transfer of a nano-encapsulated phase change material suspension in a cylindrical enclosure with partial heated walls," Int. Commun. Heat Mass Tran., vol. 164, p. 108812, 2025, doi: 10.1016/j.icheatmasstransfer.2025.108812.